OPEN ACCESS
IOP Publishing
Journal of Physics: Condensed Matter
J. Phys.: Condens. Matter **36** (2024) 335401 (9pp)
https://doi.org/10.1088/1361-648X/ad4a16

The dynamical bulk boundary correspondence and dynamical quantum phase transitions in the Benalcazar–Bernevig–Hughes model

Tomasz Masłowski[1] **and Nicholas Sedlmayr**[2,*]

[1] The Faculty of Mathematics and Applied Physics, Rzeszów University of Technology, al. Powstańców Warszawy 6, 35-959 Rzeszów, Poland
[2] Institute of Physics, M. Curie-Skłodowska University, 20-031 Lublin, Poland

E-mail: ndsedlmayr@gmail.com

Received 29 January 2024, revised 21 April 2024
Accepted for publication 10 May 2024
Published 22 May 2024

Abstract

In this article we demonstrate that dynamical quantum phase transitions (DQPTs) occur for an exemplary higher order topological insulator, the Benalcazar–Bernevig–Hughes model, following quenches across a topological phase boundary. A dynamical bulk boundary correspondence is also seen both in the eigenvalues of the Loschmidt overlap matrix and the boundary return rate. The latter is found from a finite size scaling analysis for which the relative simplicity of the model is crucial. Contrary to the usual two dimensional case the DQPTs in this model show up as cusps in the return rate, as for a one dimensional model, rather than as cusps in its derivative as would be typical for a two dimensional model. We explain the origin of this behaviour.

Keywords: quantum dynamics, topological insulators, bulk boundary correspondence

1. Introduction

In the last ten years an analogue of quantum phase transitions which can occur in time following sudden quenches has been developed. These dynamical quantum phase transitions (DQPTs) [1–3] have become one method for systematically studying the non-equilibrium behaviour of a wide variety of quantum systems. Although initial studies suggested a close connection between the equilibrium phase diagram and DQPTs, interestingly in general no such connection holds [4–12] allowing DQPTs to be a window into genuinely non-equilibrium phenomena. Following the introduction of the concept a large amount of theoretical work has followed [1, 13–21, 23–44], along with several experiments on ion trap, cold atom, and quantum simulator platforms [45–51]. Amongst other developments extensions to finite temperatures and open or dissipative systems have been made [22, 52–61]. Many studies remain focused on spin chains and one dimension, though multi-band models [11, 30, 43, 62, 63], and to higher dimensional systems [6, 43, 64–67] have also been considered. Connections have also been considered between DQPTs and other phenomena, for example the entanglement entropy [22], string order parameters [68], the characteristic function of work [55, 69], crossovers in the quasiparticle spectra [20], and out of time ordered correlators [70–73].

DQPTs have been shown to occur in many different examples of topological matter [6, 9, 23, 30, 43, 74–78]

* Author to whom any correspondence should be addressed.

which is also a recent growth industry [79–81]. One of the interesting phenomena seen in topological materials is the relation between the bulk topology and protected edge states of one dimension lower [82], this is referred to as the bulk-boundary correspondence. In a higher order topological insulator the edge modes have a dimension lower than the bulk by more than one [83–94]. Dynamical order parameters for DQPTs have been found [53, 54, 95, 96] and a dynamical bulk boundary correspondence has also been seen [22, 30], including in higher order topological matter [43].

In this work we focus on a paradigmatic example of a two dimensional higher order topological insulator: the Benalcazar–Bernevig–Hughes (BBH) model [86, 87]. This allows us to derive expressions which determine the DQPTs analytically, and obtain numerical solutions sufficient for performing a finite sized scaling analysis. We show that this two dimensional model can also exhibit behaviour characteristic of one dimensional DQPTs.

In section 2 we introduce the concept of DQPTs and the methods for calculations, and in section 3 we introduce the BBH model, describing its symmetry properties, spectra, and topological phase diagram. Section 2 contains the results on DQPTs and the dynamical bulk-boundary correspondence, following which we conclude.

2. Dynamical quantum phase transitions

DQPTs are defined using the overlap between an initial state $|\Psi_0\rangle$ and this state time evolved by a Hamiltonian $\hat{H}^1$. This overlap is called the Loschmidt echo [1]

$$L(t) = \langle\Psi_0|e^{-i\hat{H}^1 t}|\Psi_0\rangle\,. \tag{1}$$

For complex t the boundary part of $L(t)$ at $\mathrm{Im}(t)\to\infty$ is equivalent to the standard partition function. This corresponds to a quench scenario where one can consider the initial state as the ground state of a Hamiltonian $\hat{H}^0$ which is then suddenly changed and the system is time evolved with a different Hamiltonian $\hat{H}^1$. Properties of the time evolution can therefore be related to the properties of $\hat{H}^0$ and $\hat{H}^1$.

One can then define a 'free energy' called the return rate

$$l_0(t) = \lim_{N\to\infty} l_N(t) = -\lim_{N\to\infty}\frac{1}{N}\ln|L(t)|\,, \tag{2}$$

which has non-analyticities at zeroes of the Loschmidt echo. Here N is the total number of sites in the system. In analogy to a standard quantum phase transition these non-analyticities are referred to as DQPTs. In one dimensional systems the non-analyticities occur at critical times when the zeroes of $L(t)$ in the complex plane cross the real time axis [1], known as Fisher zeroes. In the bulk the line of Fisher zeroes can be parameterised by momenta. At a critical momenta the line can cross the real axis and a DQPT occurs. In two dimensions the situation is more complicated as the Fisher zeroes now form a plane and the critical region which crosses the real axis is extended over a finite range of time [6]. In that case where the density of these zeroes diverges a cusp forms in the derivative of the return rate.

For our purposes a convenient representation for the Loschmidt echo is [23, 97–99]

$$L(t) = \det\underbrace{\left[\mathbb{I} - \mathcal{C} + \mathcal{C}e^{i\mathcal{H}^1 t}\right]}_{\equiv \boldsymbol{M}(t)} \tag{3}$$

where $\mathbb{I}$ the identity matrix, $\mathcal{C}$ is the correlation matrix with $\mathcal{C}_{ij} = \langle\Psi_0|c_i^\dagger c_j|\Psi_0\rangle$ for some complete basis set of creation operators $\{c_j^\dagger\}$, and $\mathcal{H}^1$ is the Hamiltonian density of $\hat{H}^1$ written in the same basis. In terms of the eigenvalues $\lambda_i(t)$ of the matrix $\boldsymbol{M}(t)$ one finds

$$L(t) = \prod_i \lambda_i(t)\,, \tag{4}$$

and

$$l_N(t) = -\frac{1}{N}\sum_i \ln|\lambda_i(t)|\,. \tag{5}$$

We also define the required derivative

$$d_N(t) \equiv \dot{l}_N(t) = -\frac{1}{N}\sum_i\left|\frac{\dot{\lambda}_i(t)}{\lambda_i(t)}\right|\,, \tag{6}$$

which in terms of the Loschmidt matrix is

$$d_N(t) \equiv \dot{l}_N(t) = -\frac{1}{N}\mathrm{Re}\left(\mathrm{tr}\left[\dot{\boldsymbol{M}}(t)\boldsymbol{M}^{-1}(t)\right]\right)\,. \tag{7}$$

In the thermodynamic limit we write $d_0(t) = \lim_{N\to\infty} d_N(t)$.

In equilibrium the bulk-boundary correspondence relates the bulk topology to the existence of edge modes [82]. For DQPTs a dynamical bulk boundary correspondence has been discovered which relates the change in topology between the initial state and the time evolving Hamiltonian to boundary contributions to the return rate [23, 30, 43]. The boundary return rate in one dimension, $l_B^{1D}(t)$, can be found from

$$l_N^{1D}(t) \sim l_0^{1D}(t) + \frac{l_B^{1D}(t)}{N}\,. \tag{8}$$

In the simplest scenario a quench from the topologically non-trivial to the topologically trivial case results in periodically appearing and vanishing plateaus in $l_B^{1D}(t)$ between critical times. These plateaus can be directly related to zero eigenvalues of the Loschmidt matrix which become pinned to zero between alternating critical times, when the spectrum of the Loschmidt matrix becomes gapless, thus demonstrating the close analogy to the equilibrium bulk-boundary correspondence. Indeed the number of zero eigenvalues is related to the topological indices of the initial and time evolving Hamiltonians, though this connection is not necessarily that direct when larger topological indices are involved [23] or for cases where DQPTs can occur for quenches within a topologically non-trivial phase [30].

In two dimensions a similar dynamical bulk boundary correspondence has been seen in intrinsic and extrinsic higher order topological insulators [43]. In that case the critical times become extended into regions of finite duration, but pinned

zero modes of the Loschmidt matrix can still be seen between successive critical regions. In principle one would expect also plateaus in an appropriately defined boundary return rate would also occur. However the models previously studied were too complex for good enough data to be produced to determine this. One principle goal of this work is to fill this gap by focusing on a minimal model of a higher order topological insulator. If N is the total number of atoms in the two dimensional lattice then we may expect scaling of the form

$$l_N(t) \sim l_0(t) + \frac{l_B(t)}{\sqrt{N}}. \tag{9}$$

The boundary contribution at a definite system size can be directly compared to the contribution from the $\tilde{n}$ eigenvalues $\lambda_i(t)$ which become pinned to zero:

$$l_N(t) - l_0(t) \approx -\frac{1}{N}\sum_{n=0}^{\tilde{n}-1} \ln|\lambda_n(t)|. \tag{10}$$

For the model we will focus on here the topological regime contains four corner states and we find that $\tilde{n} = 4$.

3. The Benalcazar–Bernevig–Hughes model

The BBH model is a minimal four band model given by

$$\mathcal{H}_m = J\vec{\Gamma}\cdot\vec{d}^m_{\vec{k}}, \tag{11}$$

where $\vec{\Gamma}$ is a vector containing four 4×4 matrices. The matrices are given by $\Gamma_k = -\tau_2\sigma_k$ for $k = 1,2,3$, and by $\Gamma_4 = \tau_1\sigma_0$. The momentum dependent vector defining the Hamiltonian is

$$\vec{d}^m_{\vec{k}} = \begin{pmatrix} \sin k_y \\ m + \cos k_y \\ \sin k_x \\ m + \cos k_x \end{pmatrix}. \tag{12}$$

J is an overall energy scale of the hopping terms and we will set everywhere $J = 1$ and $\hbar = 1$. This is an intrinsic higher order topological insulator with four corner modes, see figure 1 for the spectrum as a function of m. The bulk eigenenergies are two-fold degenerate and are given by

$$\pm\epsilon^m_{k_x,k_y} = \pm\sqrt{2}\sqrt{1 + m^2 + m(\cos k_x + \cos k_y)}. \tag{13}$$

This model has several symmetries. First a global particle hole symmetry $\mathcal{C} = \tau_3 \times \sigma_0\hat{K}$ satisfying $\{\mathcal{C}, \mathcal{H}_m\} = 0$ and $\mathcal{C}^2 = 1$. There is also a 'time-reversal' symmetry $\mathcal{T} = \tau_0 \times \sigma_0\hat{K}$ which satisfies $\{\mathcal{T}, \mathcal{H}_m\} = 0$ and $\mathcal{T}^2 = 1$, with $\hat{K}$ being charge conjugation. Finally there are also crystalline symmetries present, such as the mirror symmetries [87, 93]

$$\mathcal{U}_y\mathcal{H}_m(-k_x,k_y)\mathcal{U}_y^\dagger = \mathcal{H}_m(k_x,k_y) \tag{14}$$

and

$$\mathcal{U}_x\mathcal{H}_m(k_x,-k_y)\mathcal{U}_x^\dagger = \mathcal{H}_m(k_x,k_y). \tag{15}$$

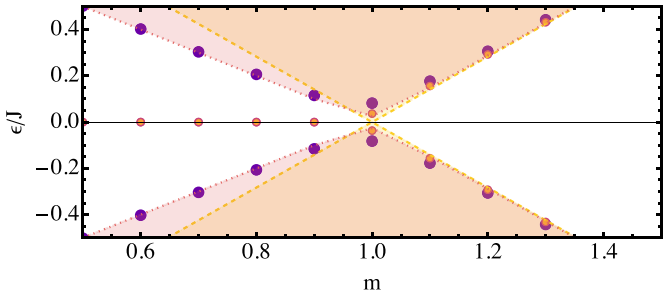

Figure 1. The spectrum of the BBH model as a function of m. Shown are the lowest 6 eigenenergies for the square lattice with open boundary conditions (circles) for $N = 60^2$. The bulk gap is shown as a shaded orange region, and the gapped one dimensional edge modes on the edge of the square lattice are shown as the purple shaded region.

Here $\mathcal{U}_y = \tau_1\sigma_3$ and $\mathcal{U}_x = \tau_1\sigma_1$. The other crystalline symmetry is a four fold rotational symmetry

$$\mathcal{U}_4\mathcal{H}_m(-k_y,k_x)\mathcal{U}_4^\dagger = \mathcal{H}_m(k_x,k_y) \tag{16}$$

with

$$\mathcal{U}_4 = \begin{pmatrix} 0 & 0 & 1 & 0 \\ 0 & 0 & 0 & 1 \\ 0 & -1 & 0 & 0 \\ 1 & 0 & 0 & 0 \end{pmatrix} \tag{17}$$

and $\mathcal{U}_4^4 = -1$. The crystalline symmetries become broken at the edges of the model, gapping the one dimensional edge modes and resulting in the corner modes. Due to the four fold rotational symmetry it is clear that there must be four corner modes for this model.

For all examples shown throughout this article we choose $m = 0.5$ for the topologically non-trivial phase and $m = 1.5$ for the topologically trivial phase. No results depend qualitatively on the exact values used. For ease of reference we label the topologically non-trivial phase by an invariant $\nu = 1$ and the topologically trivial phase by an invariant $\nu = 0$.

4. Results

From equation (3) one can readily derive the bulk expression for the Loschmidt matrix for the system with periodic boundary conditions, for more details see appendix A. For a quench from $\mathcal{H}^0 = \mathcal{H}_m$ to $\mathcal{H}^1 = \mathcal{H}_{m'}$ this results in the Loschmidt amplitude:

$$L(t) = \prod_{\vec{k}}\left[\cos\left(\epsilon^{m'}_{\vec{k}}t\right) + i\cos\delta\phi_{\vec{k}}\sin\left(\epsilon^{m'}_{\vec{k}}t\right)\right]^2, \tag{18}$$

where

$$\cos\delta\phi_{\vec{k}} = -\frac{\vec{d}^m_{\vec{k}}\cdot\vec{d}^{m'}_{\vec{k}}}{\epsilon^m_{\vec{k}}\epsilon^{m'}_{\vec{k}}}. \tag{19}$$

This is closely related to the standard expression for a two band topological insulator [6], but we note is not a general expression for a four band model [30, 43].

The first condition for the critical times to occur is for $\cos\delta\phi_{\vec{k}} = 0$ which happens for the critical momenta satisfying

$$\cos k_x^* + \cos k_y^* = -2\frac{1+mm'}{m+m'}. \tag{20}$$

This can be solved for real momenta only if

$$m(1-m') > (1-m'). \tag{21}$$

Hence for $m' > 1$ one needs $m < 1$ and vice versa. These are precisely those quenches which cross the equilibrium phase boundary, as one would expect for a simple two band topological insulator [6]. The critical times are then, for $n = 0, 1, 2, \ldots$, given by

$$t_c = \frac{\pi(2n+1)}{2\epsilon^{m'}_{k_x^*,k_y^*}} = \frac{\pi(2n+1)}{2\sqrt{2}}\sqrt{\frac{m+m'}{(m'^2-1)(m'-m)}}. \tag{22}$$

In this case, because the condition for the momenta (20) appears as it does in the energy, the plane of Fisher zeroes collapses to a line, and there is a single critical time as in one dimension. From (22) it is clear that the Fisher zeroes will only cross the real axis when either $m' > 1$ and $m' > m$, or when $m' < 1$ and $m' < m$, assuming that both m' and m are positive.

The Fisher zeroes themselves can also be easily found from (18):

$$\mathrm{Re}[t] = \frac{\pi(2n+1)}{2\epsilon^{m'}_{\vec{k}}}, \tag{23}$$

$$\mathrm{Im}[t] = \frac{\mathrm{arctanh}\left[\cos\delta\phi_{\vec{k}}\right]}{\epsilon^{m'}_{\vec{k}}}, \tag{24}$$

see figures 2 for examples. If the condition (21) is not met then the Fisher zeroes do not cross the real time axis. Here we show exemplary quenches which cross the equilibrium phase boundary in the two different directions.

For the derivative of the return rate we expect a sudden jump at the critical times, which can be seen in figures 3 and 4 for the quenches from topologically trivial to non-trivial and vice versa. This corresponds to a cusp in the return rate itself as is seen in one dimensional models. As the entire area of Fisher zeroes is collapsed onto a single curve for the BBH model this is to be expected. For the bulk there is no qualitative difference between these two possible quench scenarios, though specific details do of course change.

4.1. The dynamical bulk-boundary correspondence

We now turn to the boundary contributions. In figure 5 we show the boundary return rate l_B extracted from a finite scaling analysis for system sizes $\sqrt{N} \in \{30, 35, 40, 45, 50, 55, 60\}$, see equation (9). As we know $l_0(t)$ we can extract the boundary term $l_B(t)$ by a normal fitting procedure, see appendix B.

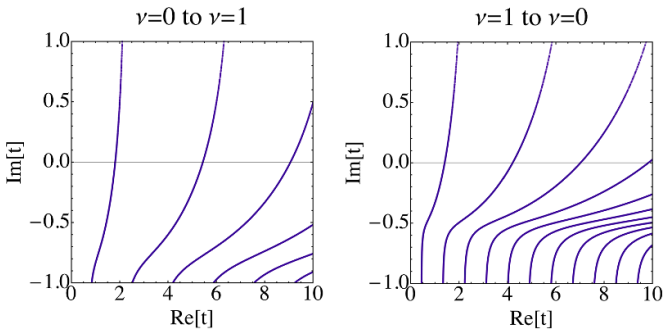

Figure 2. The Fisher zeroes in the complex t plane for quenches across the equilibrium topological phase boundary. Critical times when the zeroes cross the real axis are clearly visible. In this case each line is parameterised by both k_x and k_y and so there are many zeroes at each point. The quench $\nu : 0 \to 1$ is for $m = 1.5$ and $m' = 0.5$. The quench $\nu : 1 \to 0$ is for $m = 0.5$ and $m' = 1.5$.

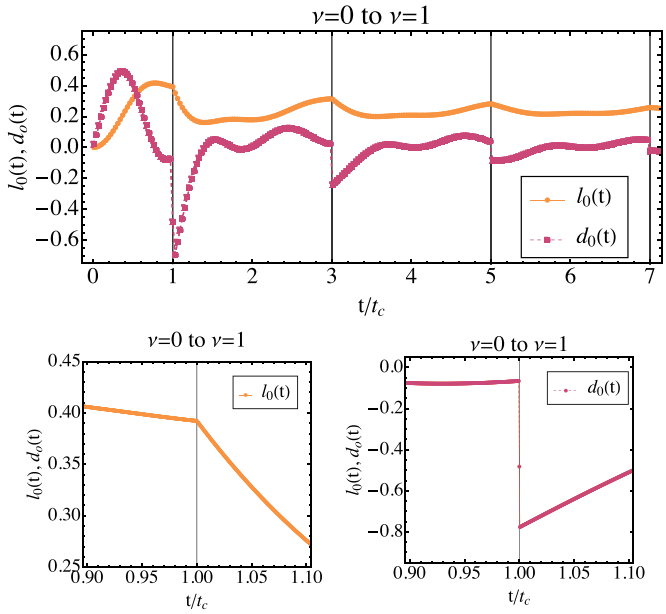

Figure 3. The return rate and its derivative for a quench from the topologically trivial to the topologically non-trivial phase. A jump in $d_0(t)$ at t_c is clearly visible, as well as a cusp in the return rate itself. The lower panels show a zoom in for the first critical time, demonstrating the cusp in the return rate and the discontinuity in its derivative. The quench parameters are $m = 1.5$ and $m' = 0.5$.

$N = 60^2$ is the largest system size we were able to reach, placing some limitations on the scaling analysis. We recall that in a one-dimensional topological system the dynamical bulk-boundary effect corresponds to a plateau forming for quenches into the topologically non-trivial phase [23, 30]. This plateau appears and disappears between successive critical times. For the opposite quench direction only small fluctuations in $l_B(t)$ occur. Similarly here we find only relatively small fluctuations in $l_B(t)$ for the quench from $\nu : 1 \to 0$, see figure 5. For the quench from $\nu : 0 \to 1$ a larger plateau-like structure can be seen to form between the first two critical times. However between the next critical times it is slow to decay, and already after the third critical time it is less clear, though $l_B(t)$ remains

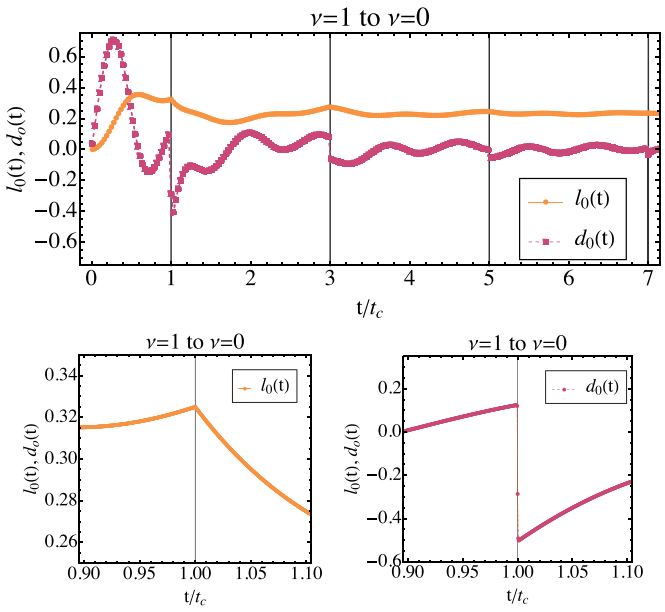

Figure 4. The return rate and its derivative for a quench from the topologically non-trivial to the topologically trivial phase. A jump in $d_0(t)$ at t_c is clearly visible, as well as a cusp in the return rate itself. The lower panels show a zoom in for the first critical time, demonstrating the cusp in the return rate and the discontinuity in its derivative. The quench parameters are $m = 0.5$ and $m' = 1.5$.

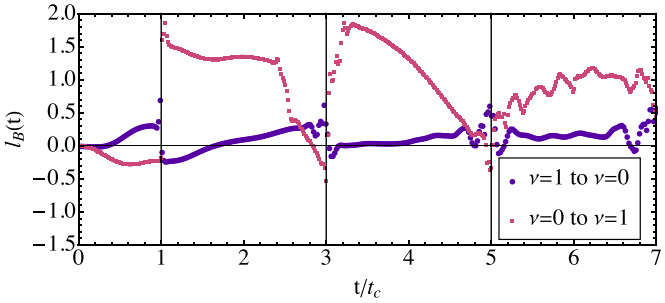

Figure 5. The boundary return rate $l_B(t)$ extracted from a finite size scaling analysis for system sizes $\sqrt{N} \in \{30, 35, 40, 45, 50, 55, 60\}$, see equation (9). As expected from the dynamical bulk-boundary correspondence the quench into the non-trivial phase shows large features between successive critical times. For a detailed discussion see the main text.

larger for the quench to the topologically non-trivial phase compared to the quench into the trivial phase as predicted. The origin of the plateau can be traced to the Loschmidt matrix eigenvalues, it is caused by zero eigenvalues which appear and disappear between successive critical times when the gap in the Loschmidt matrix spectrum closes [22, 30]. It is this behaviour which is referred to as the dynamical bulk-boundary correspondence. To clarify the situation here we now turn to the eigenvalues of the Loschmidt matrix.

In figure 6 the lowest eigenvalues of the Loschmidt matrix are shown for the two quenches considered and for systems with both open and periodic boundary conditions. As

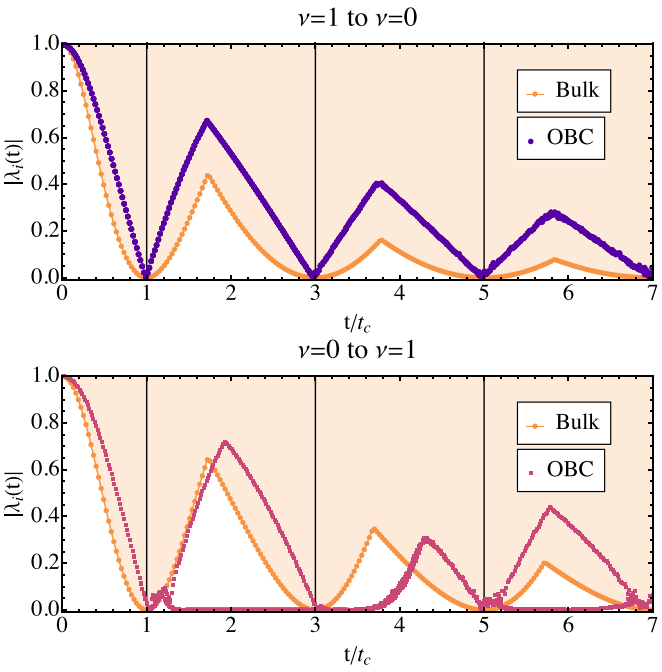

Figure 6. The eigenvalues of the Loschmidt matrix, see equations (3) and (4). Shown is the lowest eigenvalue for a bulk system of size $N = 200^2$ implemented using periodic boundary conditions, and the results for an open system using open boundary conditions (OBC) of size $N = 60^2$. The shaded region is the region in which bulk eigenvalues exist. The upper panel shows the quench form the non-trivial to the trivial phase and no zero eigenvalues occur. The lower panel shows the quench from the trivial to the non-trivial phase and four eigenvalues become pinned to zero between successive critical times t_c, in agreement with the dynamical bulk-boundary correspondence.

predicted by the dynamical bulk-boundary correspondence four zero eigenvalues occur between alternate critical times, but only for the quench into the non-trivial phase. The slow decay of the boundary return rate for the quench $\nu : 0 \to 1$ is explained by the slow increase in the absolute value of the eigenvalues which were zero for $t_c < t < 3t_c$. The discrepancy between the lowest eigenvalues for the open and periodic systems is caused by the existence of gapped one dimensional edge states which exist on the boundary of the open system, but which naturally do not occur for periodic boundary conditions.

We can compare the contribution to the return rate of just the lowest eigenvalues for the quench $\nu : 0 \to 1$ to the boundary return rate. According to the dynamical bulk-boundary correspondence

$$l_B(t) \approx \sqrt{N}(l_N(t) - l_0(t)) \approx -\frac{1}{\sqrt{N}} \sum_{i=0}^{3} \ln|\lambda_i(t)|. \qquad (25)$$

In figure 7 we compare these two quantities. Some qualitative agreement is visible, though at the system sizes we can achieve there is no quantitative agreement possible.

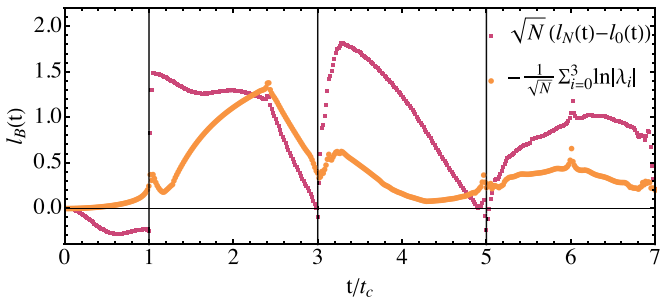

Figure 7. A comparison of the boundary contribution to the return rate extracted directly from $l_N(t)$ for $N = 60^2$ and from the lowest Loschmidt eigenvalues, see equation (25).

5. Discussion and conclusions

In this work we investigated DQPTs and the dynamical bulk-boundary correspondence for an exemplary two dimensional higher order topological insulator. The relative simplicity of this model allows us to obtain higher quality data than has previously been obtained for DQPTs in more complicated higher order topological insulators. This simplicity also leads to a collapse of the area of Fisher zeroes onto lines of Fisher zeroes in the complex time plane, leading to DQPT behaviour which is characteristic of one dimensional rather than two dimensional topological models. Correspondingly we find that cusps occur in the return rate, and discontinuities occur in its derivative, at periodic critical times for quenches across a topological phase boundary.

We also see clear evidence of a dynamical bulk-boundary correspondence in the behaviour of the eigenvalues of the Loschmidt matrix. At critical times the spectrum of the Loschmidt matrix becomes gapless, and between alternate critical times there are 'in-gap' eigenvalues pinned to zero, but only for quenches into the topologically non-trivial regime. These zeroes give rise to alternating plateaus in the boundary contribution to the return rate which we try to extract from a scaling analysis, comparing this to the boundary contribution at a specific system size and to the contribution form the zero eigenvalues. Here agreement is not perfect due to finite size errors. A systematic study of the dynamical bulk-boundary correspondence for different models and for quenches between a wider range of topological phases, and also of the origin of the Loschmidt zero eigenvalues, are interesting avenues to follow up.

Data availability statement

The data that support the findings of this study are openly available at the following URL/DOI: https://zenodo.org/records/10571375 [100].

Acknowledgments

This work was supported by the National Science Centre (NCN, Poland) Under the Grant 2019/35/B/ST3/03625.

Appendix A. Further details of the calculations

Here we give the Hamiltonian in real space, which follows from a standard Fourier transform of equation (11). The lattice is square, and the subspace could be, for example, a combination of spin and orbital spaces. The Hamiltonian is

$$H = \sum_l \Psi_l^\dagger \vec{\Gamma}\cdot\vec{d}_m \Psi_l + \sum_{\langle l,l'\rangle} \Psi_l^\dagger \vec{\Gamma}\cdot\vec{d}_{l,l'}\Psi_{l'} \tag{A1}$$

with $\Psi_n^\dagger = (c_{l1}^\dagger, c_{l2}^\dagger, c_{l3}^\dagger, c_{l4}^\dagger)$ and $c_{lj}^\dagger$ is a fermionic creation operator at site l with a subspace label j. $\langle l,l'\rangle$ refers to pairs of nearest neighbours on a square lattice. The vectors are

$$\vec{d}_m = m\,(0,1,0,1)\,, \text{and} \tag{A2}$$

$$\vec{d}_{l,l'} = \frac{1}{2}\,(i y_{l,l'}, |y_{l,l'}|, i x_{l,l'}, |x_{l,l'}|)\,, \tag{A3}$$

where $x_{l,l'} = \hat{x}\cdot[\vec{r}_{l'} - \vec{r}_l]$ and $y_{l,l'} = \hat{y}\cdot[\vec{r}_{l'} - \vec{r}_l]$ with $\vec{r}_l$ the position of site l.

For periodic boundary conditions the Loschmidt amplitude can be found analytically. In this case after a Fourier transform one finds the matrix $\mathbf{M}(t)$ is block diagonal resulting with each block labelled by a momentum $\vec{k}$. By working in the basis used for (11) one can calculate the eigenstates of $\mathcal{H}^0$ from which we can write $\mathcal{C}$. For a quench from $\mathcal{H}^0 = \mathcal{H}_m$ to $\mathcal{H}^1 = \mathcal{H}_{m'}$ we require the following matrices labelled by momenta:

$$\mathcal{C}_{\vec{k}} = \frac{1}{2}\begin{pmatrix} 1 & 0 & -\frac{m+e^{ik_x}}{\epsilon_{\vec{k}}^m} & -\frac{m+e^{ik_y}}{\epsilon_{\vec{k}}^m} \\ 0 & 1 & \frac{m+e^{-ik_y}}{\epsilon_{\vec{k}}^m} & -\frac{m+e^{-ik_x}}{\epsilon_{\vec{k}}^m} \\ -\frac{m+e^{-ik_x}}{\epsilon_{\vec{k}}^m} & \frac{m+e^{ik_y}}{\epsilon_{\vec{k}}^m} & 1 & 0 \\ -\frac{m+e^{-ik_y}}{\epsilon_{\vec{k}}^m} & -\frac{m+e^{ik_x}}{\epsilon_{\vec{k}}^m} & 0 & 1 \end{pmatrix}, \tag{A4}$$

and

$$e^{i\mathcal{H}_{\vec{k}}^1 t} = \begin{pmatrix} \cos\left(\epsilon_{\vec{k}}^{m'} t\right) & 0 & i\gamma_{\vec{k}}(k_x) & i\gamma_{\vec{k}}(k_y) \\ 0 & \cos\left(\epsilon_{\vec{k}}^{m'} t\right) & -i\gamma_{\vec{k}}(-k_y) & i\gamma_{\vec{k}}(-k_x) \\ i\gamma_{\vec{k}}(-k_x) & -i\gamma_{\vec{k}}(k_y) & \cos\left(\epsilon_{\vec{k}}^{m'} t\right) & 0 \\ i\gamma_{\vec{k}}(-k_y) & i\gamma_{\vec{k}}(k_x) & 0 & \cos\left(\epsilon_{\vec{k}}^{m'} t\right) \end{pmatrix} \tag{A5}$$

where $\gamma_{\vec{k}}(q) = (m' + e^{iq})\sin(\epsilon_{\vec{k}}^{m'} t)/\epsilon_{\vec{k}}^{m'}$. Then $\mathcal{C}$ is the block diagonal matrix with $\mathcal{C}_{\vec{k}}$ as the diagonal blocks, and similarly for $e^{i\mathcal{H}^1 t}$.

Appendix B. Finite size scaling

To find the boundary return rate l_B we perform a finite scaling analysis for system sizes $\sqrt{N} \in \{30, 35, 40, 45, 50, 55, 60\}$. We fit our data for $l_N(t)$ to

$$l_{\text{fit}}(t) = l_0(t) + \frac{l_B(t)}{\sqrt{N}} + \frac{A(t)}{N} \tag{B1}$$

where for $l_0(t)$ we use our bulk result, $l_B(t)$ is the term we want to find, and $A(t)$ is the next order term and is an additional

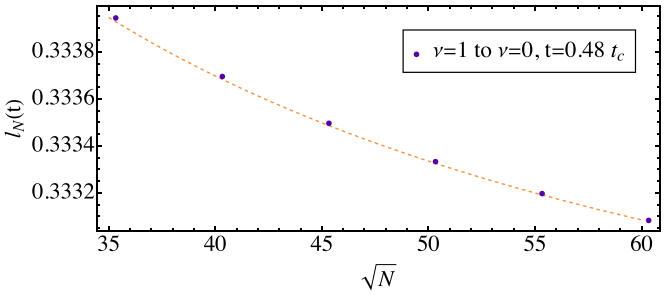

Figure 8. An example of the scaling of $l_N(t)$ for $\sqrt{N} \in \{30, 35, 40, 45, 50, 55, 60\}$ compared to $l_{\text{fit}}(t)$ (dashed line), see equation (B1).

fitting parameter which improves the fits at the system sizes we can reach. This is performed for each quench at each time step. An example of $l_{\text{fit}}(t)$ compared to $l_N(t)$ at a particular time is shown in figure 8.

ORCID iDs

Tomasz Masłowski https://orcid.org/0000-0003-4267-2246
Nicholas Sedlmayr https://orcid.org/0000-0002-8166-7485

References

[1] Heyl M, Polkovnikov A and Kehrein S 2013 Dynamical quantum phase transitions in the transverse-field ising model *Phys. Rev. Lett.* **110** 135704
[2] Heyl M 2018 Dynamical quantum phase transitions: a review *Rep. Prog. Phys.* **81** 054001
[3] Sedlmayr N 2019 Dynamical phase transitions in topological insulators *Acta Phys. Pol.* A **135** 1191
[4] Vajna S and Dóra B 2014 Disentangling dynamical phase transitions from equilibrium phase transitions *Phys. Rev.* B **89** 161105(R)
[5] Andraschko F and Sirker J 2014 Dynamical quantum phase transitions and the Loschmidt echo: a transfer matrix approach *Phys. Rev.* B **89** 125120
[6] Vajna S and Dóra B 2015 Topological classification of dynamical phase transitions *Phys. Rev.* B **91** 155127
[7] Karrasch C and Schuricht D 2017 Dynamical quantum phase transitions in the quantum potts chain *Phys. Rev.* B **95** 075143
[8] Jafari R and Johannesson H 2017 Decoherence from spin environments:Loschmidt echo and quasiparticle excitations *Phys. Rev.* B **96** 224302
[9] Jafari R and Johannesson H 2017b Loschmidt echo revivals: critical and noncritical *Phys. Rev. Lett.* **118** 015701
[10] Cheraghi H and Mahdavifar S 2018 Ineffectiveness of the Dzyaloshinskii–Moriya interaction in the dynamical quantum phase transition in the ITF model *J. Phys.: Condens. Matter* **30** 42LT01
[11] Jafari R 2019 Dynamical quantum phase transition and quasi particle excitation *Sci. Rep.* **9** 2871
[12] Wrześniewski K, Weymann I, Sedlmayr N and Domański T 2022 Dynamical quantum phase transitions in a mesoscopic superconducting system *Phys. Rev.* B **105** 094514
[13] Karrasch C and Schuricht D 2013 Dynamical phase transitions after quenches in nonintegrable models *Phys. Rev.* B **87** 195104
[14] Sharma S, Russomanno A, Santoro G E and Dutta A 2014 Loschmidt echo and dynamical fidelity in periodically driven quantum systems *Europhys. Lett.* **106** 67003
[15] Heyl M 2014 Dynamical quantum phase transitions in systems with broken-symmetry phases *Phys. Rev. Lett.* **113** 205701
[16] Heyl M 2015 Scaling and universality at dynamical quantum phase transitions *Phys. Rev. Lett.* **115** 140602
[17] Sharma S, Suzuki S and Dutta A 2015 Quenches and dynamical phase transitions in a nonintegrable quantum Ising model *Phys. Rev.* B **92** 104306
[18] Halimeh J C and Zauner-Stauber V 2017 Dynamical phase diagram of quantum spin chains with long-range interactions *Phys. Rev.* B **96** 134427
[19] Homrighausen I, Abeling N O, Zauner-Stauber V and Halimeh J C 2017 Anomalous dynamical phase in quantum spin chains with long-range interactions *Phys. Rev.* B **96** 104436
[20] Halimeh J C, Van Damme M, Zauner-Stauber V and Vanderstraeten L 2020 Quasiparticle origin of dynamical quantum phase transitions *Phys. Rev. Res.* **2** 033111
[21] Shpielberg O, Nemoto T and Caetano J 2018 Universality in dynamical phase transitions of diffusive systems *Phys. Rev.* E **98** 052116
[22] Sedlmayr N, Jaeger P, Maiti M and Sirker J 2018 Bulk-boundary correspondence for dynamical phase transitions in one-dimensional topological insulators and superconductors *Phys. Rev.* B **97** 064304
[23] Sedlmayr N, Fleischhauer M and Sirker J 2018 The fate of dynamical phase transitions at finite temperatures and in open systems *Phys. Rev.* B **97** 045147
[24] Zunkovic B, Heyl M, Knap M and Silva A 2018 Dynamical quantum phase transitions in spin chains with long-range interactions: merging different concepts of non-equilibrium criticality *Phys. Rev. Lett.* **120** 130601
[25] Yang K *et al* 2019 Floquet dynamical quantum phase transitions *Phys. Rev.* B **100** 085308
[26] Srivastav V, Bhattacharya U and Dutta A 2019 Dynamical quantum phase transitions in extended toric-code models *Phys. Rev.* B **100** 144203
[27] Huang Y-P, Banerjee D and Heyl M 2019 Dynamical quantum phase transitions in U(1) quantum link models *Phys. Rev. Lett.* **122** 250401
[28] Gurarie V 2019 Dynamical quantum phase transitions in the random field Ising model *Phys. Rev.* A **100** 031601(R)
[29] Abdi M 2019 Dynamical quantum phase transition in Bose-Einstein condensates *Phys. Rev.* B **100** 184310
[30] Masłowski T and Sedlmayr N 2020 Quasiperiodic dynamical quantum phase transitions in multiband topological insulators and connections with entanglement entropy and fidelity susceptibility *Phys. Rev.* B **101** 014301
[31] Puebla R 2020 Finite-component dynamical quantum phase transitions *Phys. Rev.* B **102** 220302(R)
[32] Link V and Strunz W T 2020 Dynamical phase transitions in dissipative quantum dynamics with quantum optical realization *Phys. Rev. Lett.* **125** 143602
[33] Sun G and Wei B-B 2020 Dynamical quantum phase transitions in a spin chain with deconfined quantum critical points *Phys. Rev.* B **102** 094302
[34] Rylands C and Galitski V 2020 Dynamical quantum phase transitions and recurrences in the Non-Equilibrium BCS model (arXiv:2001.10084)
[35] Trapin D, Halimeh J C and Heyl M 2021 Unconventional critical exponents at dynamical quantum phase transitions in a randomIsing chain *Phys. Rev.* B **104** 115159

[36] Yu W C, Sacramento P D, Li Y C and Lin H-Q 2021 Correlations and dynamical quantum phase transitions in an interacting topological insulator *Phys. Rev.* B **104** 085104

[37] Halimeh J C, Van Damme M, Guo L, Lang J and Hauke P 2021 Dynamical phase transitions in quantum spin models with antiferromagnetic long-range interactions *Phys. Rev.* B **104** 115133

[38] Halimeh J C, Trapin D, Van Damme M and Heyl M 2021 Local measures of dynamical quantum phase transitions *Phys. Rev.* B **104** 075130

[39] de nicola s, michailidis a a and serbyn m 2021 entanglement view of dynamical quantum phase transitions *Phys. Rev. Lett.* **126** 040602

[40] Cheraghi H and Mahdavifar S 2021 Dynamical quantum phase transitions in the 1D nonintegrable Spin-1/2 transverse field XZZ model *Ann. Phys., Lpz.* **533** 2000542

[41] Cao K, Ming Z and Tong P Dynamical quantum phase transition in quantum spin chains with gapless phases 2021 (arXiv:2106.00191)

[42] Bandyopadhyay S, Polkovnikov A and Dutta A 2021 Observing dynamical quantum phase transitions through quasilocal string operators *Phys. Rev. Lett.* **126** 200602

[43] Masłowski T and Sedlmayr N 2023 Dynamical bulk-boundary correspondence and dynamical quantum phase transitions in higher-order topological insulators *Phys. Rev.* B **108** 094306

[44] Cheraghi H and Sedlmayr N 2023 Dynamical quantum phase transitions following double quenches: persistence of the initial state vs dynamical phases *New J. Phys.* **25** 103035

[45] Jurcevic P, Shen H, Hauke P, Maier C, Brydges T, Hempel C, Lanyon B P, Heyl M, Blatt R and Roos C F 2017 Direct observation of dynamical quantum phase transitions in an interacting many-body system *Phys. Rev. Lett.* **119** 080501

[46] Fläschner N, Vogel D, Tarnowski M, Rem B S, Lühmann D S, Heyl M, Budich J C, Mathey L, Sengstock K and Weitenberg C 2018 Observation of dynamical vortices after quenches in a system with topology *Nat. Phys.* **14** 265

[47] Zhang J, Pagano G, Hess P W, Kyprianidis A, Becker P, Kaplan H, Gorshkov A V, Gong Z-X and Monroe C 2017 Observation of a many-body dynamical phase transition with a 53-qubit quantum simulator *Nature* **551** 601

[48] Guo X-Y, Yang C, Zeng Y, Peng Y, Li H-K, Deng H, Jin Y-R, Chen S, Zheng D and Fan H 2019 Observation of a dynamical quantum phase transition by a superconducting qubit simulation *Phys. Rev. Appl.* **11** 044080

[49] Smale S, He P, Olsen B A, Jackson K G, Sharum H, Trotzky S, Marino J, Rey A M and Thywissen J H 2019 Observation of a transition between dynamical phases in a quantum degenerate Fermi gas *Sci. Adv.* **5** eaax1568

[50] Nie X *et al* 2020 Experimental observation of equilibrium and dynamical quantum phase transitions viaout-of-time-ordered correlators *Phys. Rev. Lett.* **124** 250601

[51] Tian T, Yang H-X, Qiu L-Y, Liang H-Y, Yang Y-B, Xu Y and Duan L-M 2020 Observation of dynamical quantum phase transitions with correspondence in an excited state phase diagram *Phys. Rev. Lett.* **124** 043001

[52] Mera B, Vlachou C, Paunković N, Vieira V R and Viyuela O 2018 Dynamical phase transitions at finite temperature from fidelity and interferometric Loschmidt echo induced metrics *Phys. Rev.* B **97** 094110

[53] Bhattacharya U, Bandyopadhyay S and Dutta A 2017 Mixed state dynamical quantum phase transitions *Phys. Rev.* B **96** 180303(R)

[54] Heyl M and Budich J C 2017 Dynamical topological quantum phase transitions for mixed states *Phys. Rev.* B **96** 180304(R)

[55] Abeling N O and Kehrein S 2016 Quantum quench dynamics in the transverse field Ising model at nonzero temperatures *Phys. Rev.* B **93** 104302

[56] Lang J, Frank B and Halimeh J C 2018 Dynamical quantum phase transitions: a geometric picture *Phys. Rev. Lett.* **121** 130603

[57] Lang J, Frank B and Halimeh J C 2018 Concurrence of dynamical phase transitions at finite temperature in the fully connected transverse-field Ising model *Phys. Rev.* B **97** 174401

[58] Kyaw T H, Bastidas V M, Tangpanitanon J, Romero G and Kwek L-C 2020 Dynamical quantum phase transitions and non-Markovian dynamics *Phys. Rev.* A **101** 012111

[59] Starchl E and Sieberer L M 2022 Relaxation to a parity-time symmetric generalized gibbs ensemble after a quantum quench in a driven-dissipative kitaev chain *Phys. Rev. Lett.* **129** 220602

[60] Naji J, Jafari M, Jafari R and Akbari A 2022 Dissipative floquet dynamical quantum phase transition *Phys. Rev.* A **105** 022220

[61] Kawabata K, Kulkarni A, Li J, Numasawa T and Ryu S 2022 Dynamical quantum phase transitions in SYK Lind bladians (arXiv:2210.04093)

[62] Huang Z and Balatsky A V 2016 Dynamical quantum phase transitions: role of topological nodes inwave function overlaps *Phys. Rev. Lett.* **117** 086802

[63] Mendl C B and Budich J C 2019 Stability of dynamical quantum phase transitions in quenched topological insulators: from multiband to disordered systems *Phys. Rev.* B **100** 224307

[64] De Nicola S, Michailidis A A and Serbyn M 2022 Entanglement and precession in two-dimensional dynamical quantum phase transitions *Phys. Rev.* B **105** 165149

[65] Hashizume T, McCulloch I P and Halimeh J C 2022 Dynamical phase transitions in the two-dimensional transverse-field Ising model *Phys. Rev. Res.* **4** 013250

[66] Brange F, Peotta S, Flindt C and Ojanen T 2022 Dynamical quantum phase transitions in strongly correlated two-dimensional spin lattices following a quench *Phys. Rev. Res.* **4** 033032

[67] Kosior A and Heyl M 2023 Vortex loop dynamics and dynamical quantum phase transitions in 3D fermion matter (arXiv:2307.02985)

[68] Uhrich P, Defenu N, Jafari R and Halimeh J C 2020 Out-of-equilibrium phase diagram of long-range superconductors *Phys. Rev.* B **101** 245148

[69] Talkner P, Lutz E and Hanggi P 2007 Fluctuation theorems: work is not an observable *Phys. Rev.* E **75** 050102(R)

[70] Heyl M, Pollmann F and Dóra B 2018 Detecting equilibrium and dynamical quantum phase transitions in Ising chains via out-of-time-ordered correlators *Phys. Rev. Lett.* **121** 016801

[71] Chen B, Hou X, Zhou F, Qian P, Shen H, and Xu N 2020 Detecting dynamical quantum phase transition via out-of-time-order correlations in a solid-state quantum simulator (arXiv:2001.06333)

[72] Zamani S, Jafari R and Langari A 2022 Out-of-time-order correlations and Floquet dynamical quantum phase transition *Phys. Rev.* B **105** 094304

[73] Sedlmayr M, Cheraghi H and Sedlmayr N 2023 Information trapping by topologically protected edge states: scrambling and the butterfly velocity *Phys. Rev.* B **108** 184303

[74] Schmitt M and Kehrein S 2015 Dynamical quantum phase transitions in the Kitaev honeycomb model *Phys. Rev.* B **92** 075114

[75] Jafari R 2016 Quench dynamics and ground state fidelity of the one-dimensional extended quantum compass model in a transverse field *J. Phys. A: Math. Theor.* **49** 185004
[76] Jafari R, Johannesson H, Langari A and Martin-Delgado M A 2019 Quench dynamics and zero-energy modes: the case of the Creutz model *Phys. Rev.* B **99** 054302
[77] Zache T V, Mueller N, Schneider J T, Jendrzejewski F, Berges J and Hauke P 2019 Dynamical topological transitions in the massive schwinger model with a θ term *Phys. Rev. Lett.* **122** 050403
[78] Okugawa R, Oshiyama H and Ohzeki M 2021 Mirror-symmetry-protected dynamical quantum phase transitions in topological crystalline insulators *Phys. Rev. Res.* **3** 043064
[79] Hasan M Z and Kane C L 2010 Colloquium: topological insulators *Rev. Mod. Phys.* **82** 3045
[80] Chiu C K, Teo J C, Schnyder A P and Ryu S 2016 Classification of topological quantum matter with symmetries *Rev. Mod. Phys.* **88** 035005
[81] Wen X G 2017 Colloquium: zoo of quantum-topological phases of matter *Rev. Mod. Phys.* **89** 1
[82] Teo J C Y and Kane C L 2010 Topological defects and gapless modes in insulators and superconductors *Phys. Rev.* B **82** 115120
[83] Volovik G E 2010 Topological superfluid 3He-B in magnetic field and ising variable *JETP Lett.* **91** 201
[84] Sitte M, Rosch A, Altman E and Fritz L 2012 Topological insulators in magnetic fields: quantum hall effect and Edge channels with a nonquantized theta term *Phys. Rev. Lett.* **108** 126807
[85] Zhang F, Kane C L and Mele E J 2013 Surface state magnetization and chiral Edge states on topological insulators *Phys. Rev. Lett.* **110** 046404
[86] Benalcazar W A, Bernevig B A and Hughes T L 2017a Electric multipole moments, topological multipole moment pumping and chiral hinge states in crystalline insulators *Phys. Rev.* B **96** 245115
[87] Benalcazar W A, Bernevig B A and Hughes T L 2017 Quantized electric multipole insulators *Science* **357** 61
[88] Langbehn J, Peng Y, Trifunovic L, von Oppen F and Brouwer P W 2017 Reflection-symmetric second-order topological insulators and superconductors *Phys. Rev. Lett.* **119** 246401
[89] Song Z, Fang Z and Fang C 2017 (d-2)-Dimensional edge states of rotation symmetry protected topological states *Phys. Rev. Lett.* **119** 246402
[90] Schindler F, Cook A M, Vergniory M G, Wang Z, Parkin S S P, Bernevig B A and Neupert T 2018 Higher-order topological insulators *Sci. Adv.* **4** 0346
[91] Fang C and Fu L 2019 New classes of topological crystalline insulators having surface rotation anomaly *Sci. Adv.* **5** eaat2374
[92] Trifunovic L and Brouwer P W 2019 Higher-order bulk-boundary correspondence for topological crystalline phases *Phys. Rev.* X **9** 011012
[93] Trifunovic L and Brouwer P W 2021 Higher-order topological band structure *Physica Status Solidi* b **258** 2000090
[94] Xie B, Wang H-X, Zhang X, Zhan P, Jiang J-H, Lu M and Chen Y 2021 Higher-order band topology *Nat. Rev. Phys.* **3** 520
[95] Budich J C and Heyl M 2016 Dynamical topological order parameters far from equilibrium *Phys. Rev.* B **93** 085416
[96] Wang K, Qiu X, Xiao L, Zhan X, Bian Z, Yi W and Xue P 2019 Simulating dynamic quantum phase transitions in photonic quantum walks *Phys. Rev. Lett.* **122** 020501
[97] Levitov L S, Lee H and Lesovik G B 1996 Electron counting statistics and coherent states of electric current *J. Math. Phys.* **37** 4845
[98] Klich I 2003 An elementary derivation of Levitov's formula *Quantum Noise in Mesoscopic Physics* (*Series NATO Advanced Science Series* vol 97) ed Y V Nazarov (Kluwer Academic Press) pp 397–402
[99] Rossini D, Calarco T, Giovannetti V, Montangero S and Fazio R 2007 Decoherence induced by interacting quantum spin baths *Phys. Rev.* A **75** 032333
[100] Masłowski T and Sedlmayr N 2024 The dynamical bulk boundary correspondence and dynamical quantum phase transitions in the Benalcazar-Bernevig-Hughes model Zenodo (https://doi.org/10.5281/zenodo.10571375)